Evaluation of High-Rate GNSS-PPP for Monitoring Structural Health and Seismogeodesy Applications

Cemal Ozer YIGIT, Ahmet Anil DINDAR, Mert BEZCIOGLU, Turkey
Ahmed EL-MOWAFY, Australia

Key words: GNSS, High-rate GNSS PPP, Structural Health Monitoring, Seismogeodesy

SUMMARY

This study evaluates the usability of the GNSS-PPP method for structural health monitoring and seismogeodesy applications. Two test scenarios were considered. The first test scenario included monitoring hormonic oscillations in amplitude of 5 mm to 20 mm with the frequency range of 0.2 Hz to 2.5 Hz that were generated using a shaking table, which has the ability to move in one direction in a horizontal plane. The second test scenario was carried out by simulating the El-Centro Earthquake as a seismogeodesy application. The used GNSS data comprised dual-frequency observations with a 10 Hz sampling rate. GNSS-derived positioning time series were obtained by processing the data using a post-mission kinematic PPP method and results were compared, in both the frequency domain and time domain, with LVDT (Linear Variable Differential Transformer) data, taking as a reference. Results show that the high-rate GNSS PPP method can capture the frequencies of harmonic movements comparable to the LVDT. The observed amplitudes of the harmonic oscillations are slightly different from the LVDT data at the order of mm level. These results demonstrate the ability of the high-rate GNSS PPP method to reliably monitor structural and earthquake-induced vibration frequencies and amplitudes for both the structural health and seismogeodesy applications.

Evaluation of High-Rate GNSS-PPP for Monitoring Structural Health and Seismogeodesy Applications

Cemal Ozer YIGIT, Ahmet Anil DINDAR, Mert BEZCIOGLU, Turkey
Ahmed EL-MOWAFY, Australia

1. INTRODUCTION

High-rate GNSS positioning has been recognized as a powerful tool in measuring dynamic displacements of engineering structures and surface wave motion caused by large earthquakes. Real-time or post-processed relative kinematic positioning methods that require a minimum of two GNSS receivers are widely used to measure relative displacements. Numerous studies have been conducted using such relative positioning methods to measure dynamic displacements of high-rise buildings and tall slender structures (Çelebi 2000; Li et al.2006; Park et al.2008; Yigit et al.2010; Yi et al.2013), long and short-span bridges (Nakamura 2000; Roberts et al.2004; Yi et al.2013; Moschas & Stiros 2014). In addition to the full-scale monitoring studies, there is a number of experimental studies for assessing the accuracy and dynamic performance of relative positioning methods (Chan et al. 2006, Psimoulis and Stiros, 2008, Wang et al., 2011). Some shake table tests to assess the abilities of GNSS as seismometers have been performed in the past decade (Ge et al. 2000, Larson et al., 2003; Bock et al., 2004; Bilich et al., 2008; Bock et al. 2011, Shi et al., 2010; Yin et al., 2013; Hung and Rau, 2013; Guo et al., 2013;).

In recent years, high-rate PPP methods were developed (Zumberge et al.1997; Kouba & Heroux 2001), which can provide centimeter- to decimeter-level accuracy based on the processing of un-differenced observations from a single GNSS receiver employing the measurement corrections (El-Mowafy et al. 2017). PPP has been demonstrated to be a powerful and efficient method for crustal deformation monitoring (Savage et al.2004; Calais et al. 2006; Ohta et al.2008), GPS seismology (Kouba 2003; Avallone et al. 2011, Xu et al. 2013, Nie et al. 2016; Michel et al. 2017), earthquake early warning system (Li et al. 2013) and structural health monitoring (Moschas et al. 2014, Yigit 2016, Yigit and Gurlek 2017, Kaloop et al. 2018).

The purpose of this research is to investigate how precisely high-rate PPP can measure the dynamic oscillation of engineering structures and strong ground motion caused by a large earthquake. The evaluation of performance of high-rate PPP method was performed on twenty four different oscillation events and a simulation for El-Centro earthquake generated by a single-axis shake table with a mounted GNSS atenna and LVDT sensor. The PPP results obtained from each event were compared to the corresponding LVDT data in the time and frequency domain.

The rest of the paper is organized as follows: experimental setup is introduced in Section 2. In section 3, GNSS data processing is briefly presented. The experimental results are presented and discussed in Section 4. Finally, the conclusions are drawn in Section 5.

2. EXPERIMENTAL SETUP

2.1 Shake table

Dynamic motion at an arbitrary location is simulated by using the shake table instrument, which has been widely used in earthquake engineering studies. The shake table used in the experiments can move the table, shown in Figure 1 as the black flat plate where the receiver is attached, a uniaxial movement within ± 95mm. The total stroke of the table is 190 mm. The table follows either displacement or acceleration pattern, harmonic motion or single steps. The maximum velocity is limited up to 400 mm/s. The motion of the table is provided by an electric engine that can also create low vibration. The stability of the table on a metal chassis under high frequency motions are maintained by counter-weights placed on the either sides of the platform. The position of the table on the rails is controlled by a software running on a Windows computer where the controller verifies the position using an embedded LVDT under the moving table (not visible in Figure 1). The LVDT measures the position of the table at mm level accuracy with 50 sampling per second (50 Hz). The efficiency of the LVDT and the position of the moving table is regularly controlled by external measurement instruments.

Figure 1. Shake table and GNSS receiver

The motion patterns of the shake table can be arranged as harmonic and random values. The harmonic motions are function of sinusoidal wave that is described by the amplitude, frequency and number of cycles. On the other hand, the random values are described as acceleration or displacement functions. The acceleration functions are initially converted to the displacement time-history in order to see whether the peak values exceed the stroke limits. In case of exceedance, the time-history values are scaled by an optimal factor for the sake of consistency between the peak to peak scaled values and the stroke limits.

2.2 GNSS data collection

In this study, we employed two Topcon™ HiPer-Pro GNSS receivers. One GNSS antenna/receiver was mounted on the shake table (cf. Figure 1). Another GNSS antenna/receiver was installed 20 m away from the shake table at a known station and served as a reference station. The shake table experiment was conducted at the Kültür University campus in Istanbul in August 2016 and lasted approximately 136 minutes. The shake table was kept motionless for approximately 25 minutes before starting the oscillation test in order to accelerate the process of achieving an integer ambiguity-fixed and a stable float-ambiguity solution for relative positioning and PPP, respectively. The GNSS data were recorded at a 10 Hz (0.1 s) sampling rate. Both GPS and GLONASS satellite data were collected. The experiment was conducted under open-sky conditions. The selected satellite elevation cut-off angle was 10^{o}. The weather was calm when carrying out the experiment. The number of observed GPS+GLONASS satellites varied between 12 and 16 per epoch during the experiment.

2.2.1 Harmonic Oscillation Tests

Twenty four harmonic oscillation experiments using a shake table have been conducted to evaluate the performance of the high-rate relative positioning and PPP methods and to compare their results with a reference LVDT data. Table 1 summarizes these harmonic oscillation events giving their frequency and amplitude values.

Table 1. Oscillation frequency and amplitude of each event selected for this study

		Oscillation Amplitude			
		5 mm	**10 mm**	**15 mm**	**20 mm**
Oscillation Frequency	**0.2 Hz**	Event 1	Event 2	Event 3	Event 4
	0.5 Hz	Event 5	Event 6	Event 7	Event 8
	1.0 Hz	Event 9	Event 10	Event 11	Event 12
	1.5 Hz	Event 13	Event 14	Event 15	Event 16
	2.0 Hz	Event 17	Event 18	Event 19	Event 20
	2.5 Hz	Event 21	Event 22	Event 23	Event 24

2.2.2 Earthquake Simulation Test

The El-Centro earthquake occurred on on May 19, 1940 at 05:35 UTC in Southern California. The earthquake had a magnitude Mw of 6.9 and was the first major earthquake to be recorded by a strong-motion seismograph located next to a fault rupture. It was the strongest recorded earthquake to hit the Imperial Valley, and caused a widespread damage to the irrigation systems in the area. The earthquake was the result of a rupture along the Imperial Fault, with its epicenter 5 miles (8.0 km) north of Calexico, California. A surface rupture was formed during the earthquake of 40–60 km with a maximum recorded displacement of 4.5 m close to the border. The sense of movement along the rupture was almost pure strike-slip, with no vertical displacement seen.

The random values used in the experiments are selected; excerpted from a natural strong ground motion record during El Centro, California earthquake in 1940 (Figure 2). The displacement computed from the acceleration file, depicted as solid line in the figure, was scaled down in order to move the table within the stroke limits.

Figure 2. Time-history series of El-Centro earthquake record used in the experiment

A popular record in the earthquake studies is El-Centro North-South component (1940). This record is used in this study. The frequency content of the record is narrow-banded as illustrated in Figure 3. The motion is smooth in the transitions and the reverse cyclic motions are not so severe, such that the general waveform of the displacement is not complex.

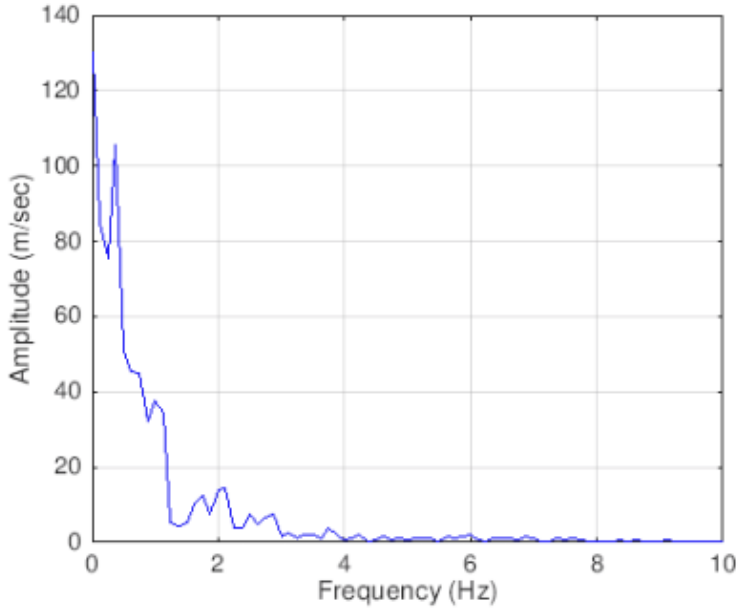

Figure 3. Frequency content of the El-Centro earthquake record used in the experiment

3. DATA PROCESSING

3.1 Kinematic Relative Positioning

The analysis of GNSS data was performed using the Leica Geo Office (LGO) 3.0 software. In processing, a standard L1+L2 solution was employed to eliminate the ionosphere effect. Furthermore, a Hopfield tropospheric model was utilized to correct the tropospheric dry delay. GNSS integer ambiguity-fixed solution was computed. Navigation ephemeris data was used for the post-processed kinematic solution.

3.2 Kinematic PPP

The GNSS data from the rover receiver on the shake table in the PPP mode were processed in the post-mission kinematic mode using the CSRS-PPP software developed by the Geodetic Survey Division of the NRCan (NRCan-GSD). It is able to compute stand-alone positions from both single- and dual-frequency GPS+GLONASS satellite data. The CSRS-PPP is suitable for processing data sampled at 10 Hz. The accuracy of the position obtained from PPP highly depends on the accuracy of the products used. CSRS-PPP software uses different GNSS orbit and clock products (ultra-rapid, rapid and IGS-Final) depending on the time of a user's data submission and the epoch of the last observation in users' dataset (Mireault et al.2008). The reader is referred to Tetreault et al. (2005) for further details about the CSRS-PPP software.

Table 2. Processing parameters used by CSRS-PPP

Mode	Kinematic
GNSS Type	GPS+GLONASS
Observation processed	Code&Phase
Frequency observed	L1, L2
Satellite orbits	Precise (EMU-Ultra rapid)
Satellite product input	CLK-RINEX
Ionospheric model	L1&L2
Tropospheric models	-Davis(GPT) for Hydrostatic delay -Hopf (GPT) for wet delay -GMF for mapping functions
Troposphere zenith delay (TZD)	Estimated
Clock interpolation	Yes
Parameter smoothing	Yes
Reference frame	ITRF

The IGS-Final products are available 13 days after the last observation while EMU (ultra-rapid) products are generated hourly and are available 90 minutes for GPS and 120 minutes for GPS+GLONASS after the last observation. In this study, the ultra-rapid precise orbit and clock products were used where the GNSS data used in this study was processed two hours after completing the experiments. Alternatively, one can use real-time products from the IGS or commercial providers (El-Mowafy et al., 2017, El-Mowafy 2018). The processing parameters used in this study are given in Table 2.

The CSRS-PPP provides geocentric Cartesian coordinates in the ITRF (International Terrestrial Reference Frame) and ellipsoidal coordinates. These coordinates cannot be directly used in structural health monitoring (SHM) or seismogeodesy applications (Yigit 2016), and therefore need to be transformed to a local topocentric Cartesian coordinate system, which is physically feasible in terms of the separation of position and height. Therefore, the point coordinates estimated from both the CSRS-PPP and LGO 3.0 software were converted from geocentric Cartesian to the local topocentric Cartesian system (Yigit 2016). Afterwards, topocentric coordinates were projected onto the movement direction of the shake table as described in Yigit (2016).

4. RESULTS AND DISCUSSIONS

In this study, LVDT data is considered as a reference to evaluate the performance of high-rate GNSS PPP method in terms of capturing dynamic motion. A number of experiments were carried out to obtain various combinations of the oscillation characteristics. LVDT, relative positioning and PPP-derived displacement time series are shown in figure 4, consisting of harmonic oscillation events and the El-Centro earthquake simulation. It can be clearly seen that

LVDT and relative positioning-derived displacement are very much consistent, whereas the PPP-derived displacement exhibit low frequency (long period) fluctuation other than the given harmonic oscillation (see events 5 to 8 in figure 4).

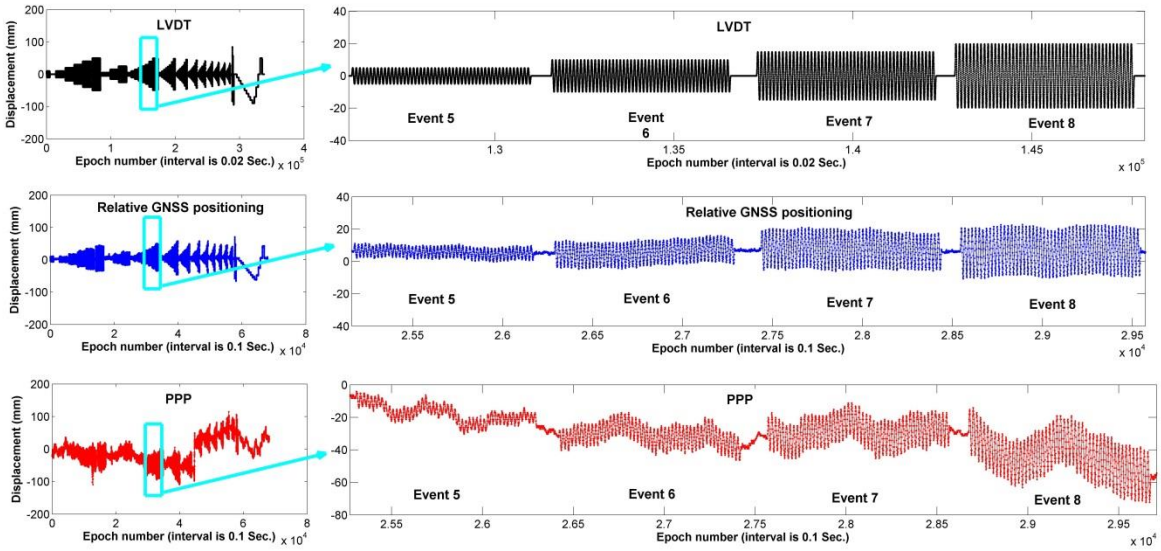

Figure 4. Overall LVDT (top panel), Relative GNSS positioning (middle panel) and PPP (bottom panel)-derived displacement (left) and zoom in for event 5 to event 8 (right). Note that relative and PPP-derived displacement is shown for the east component.

The larger variation in PPP-derived displacement time series is due to the use of float-ambiguities, where a long time is needed for reaching a converged solution. The convergence time, which represents the time to reach a stable accuracy level, is quite dependent on many factors such as the number and geometry of visible satellites, user environment and dynamics, observation quality, sampling rate and algorithm (Bisnath and Gao 2008). However, long-term fluctuation is not an issue in this study, since it is focused on the dynamic displacement over a short period of time, e.g., within 20 s to 250 s. The long-term fluctuation in PPP-derived displacement time series can be eliminated by implementing high-pass filter (Yigit 2016).

4.1 Results of Harmonic Oscillation Tests

In this study, the low-frequency components in PPP-derived time series was filtered out by applying fifth-order Butterworth high-pass filter with cut off frequency of 0.15 Hz. Figure 5 shows the LVDT, relative GNSS positioning and PPP-derived displacement time series of the events 5, 6, 7 and 8. It can be seen that in this case, PPP-derived displacements show good agreement with that of the LVDT and relative-GNSS positioning displacement. Figure 6 illustrates the FFT spectrums of the events 5 to 8. The oscillation frequencies obtained from all methods for these events are the same whereas there are slight differences in the

corresponding amplitudes. These differences can be attributed to the random noise of GNSS measurements.

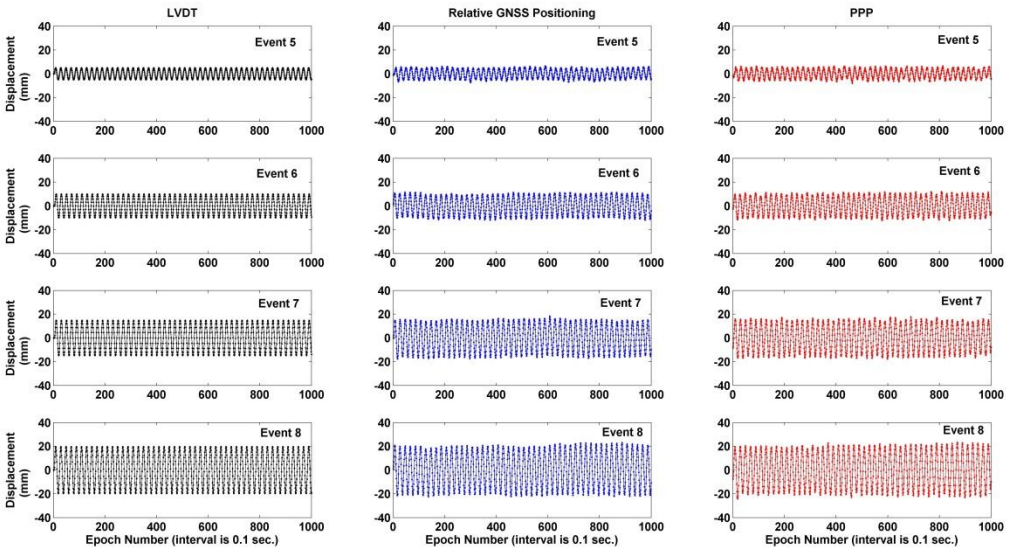

Figure 5. Time series of Event 5 to Event 8. Note that LVDT data are down-sampled to 10 Hz and PPP-derived time series is filtered.

To further examine the ability and performance of high-rate PPP method, the peak frequency and corresponding amplitude of each event obtained from FFT are summarized in Table 3. As can be seen from the table, the oscillation frequencies obtained from the three methods for each event have a good agreement. However, there are slight differences in the corresponding amplitudes. The differences in the amplitude of the oscillation frequency between the LVDT and PPP vary between 0.2 and 3.7 mm, whilst the differences between the LVDT and relative GNSS positioning are from 0.2 to 6.5 mm, as shown in Figure 7.

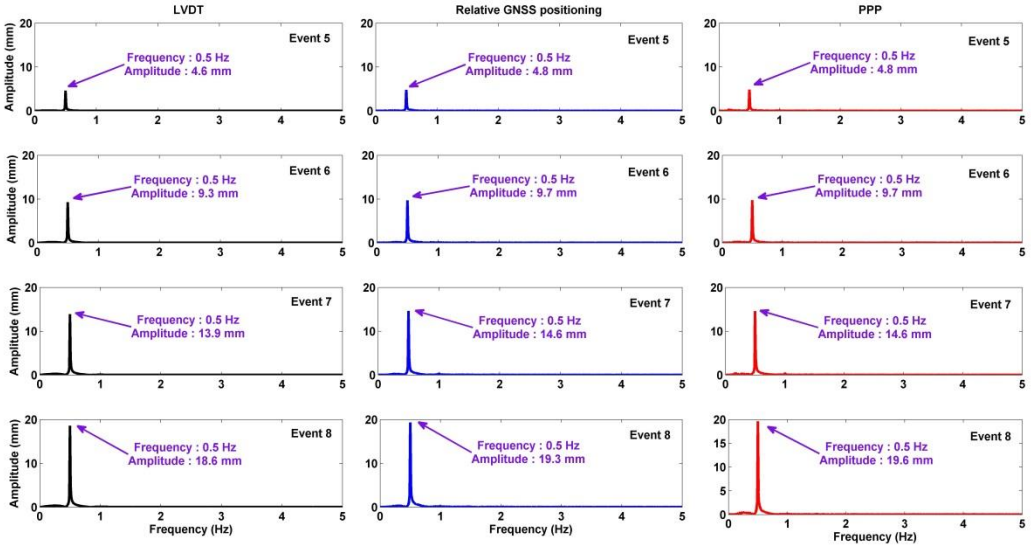

Figure 6. FFT results of filtered time series for Event 5 to Event 8 for LVDT (left), Relative GNSS positioning (middle), and PPP (right).

Table 3. Peak Frequency and amplitude for all events.

Event No	*Given Oscillation Frequency (Hz)*	*Given Oscillation Amplitude (mm)*	*LVDT*		*Relative GNSS Positioning*		*PPP (filtered)*	
			Oscillation Frequency (Hz)	*Oscillation Amplitude (mm)*	*Oscillation Frequency (Hz)*	*Oscillation Amplitude (mm)*	*Oscillation Frequency (Hz)*	*Oscillation Amplitude (mm)*
1	0.20	5	0.20	4.9	0.20	4.7	0.20	4.3
2	0.20	10	0.20	9.7	0.20	9.5	0.20	9.9
3	0.20	15	0.20	14.8	0.20	15.0	0.20	15.1
4	0.20	20	0.20	19.8	0.20	19.0	0.20	19.0
5	0.50	5	0.50	4.6	0.50	4.8	0.50	4.8
6	0.50	10	0.50	9.3	0.50	9.7	0.50	9.7
7	0.50	15	0.50	13.9	0.50	14.6	0.50	14.6
8	0.50	20	0.50	18.6	0.50	19.3	0.50	19.6
9	1.00	5	1.00	4.5	1.00	6.2	1.00	5.6
10	1.00	10	1.00	9.0	1.00	12.0	1.00	10.8
11	1.00	15	1.00	13.4	1.00	16.7	1.00	15.0
12	1.00	20	1.00	18.0	1.00	24.2	1.00	21.2
13	1.50	5	1.51	4.4	1.51	6.2	1.51	5.8
14	1.50	10	1.51	8.7	1.51	11.5	1.51	10.6
15	1.50	15	1.51	13.1	1.51	17.3	1.51	14.3
16	1.50	20	1.51	17.5	1.51	24.0	1.51	19.6
17	2.00	5	2.01	4.0	2.01	4.3	2.01	3.6
18	2.00	10	2.01	8.0	2.01	9.2	2.01	7.5
19	2.00	15	2.01	12.1	2.00	13.3	2.00	11.8
20	2.00	20	2.01	16.1	2.01	18.3	2.01	15.5
21	2.50	5	2.52	4.0	2.52	4.1	2.52	3.4

22	2.50	10	2.52	8.0	2.52	7.4	2.52	6.2
23	2.50	15	2.52	12.0	2.52	11.2	2.52	9.5
24	2.50	20	2.52	16.0	2.52	15.4	2.52	13.3

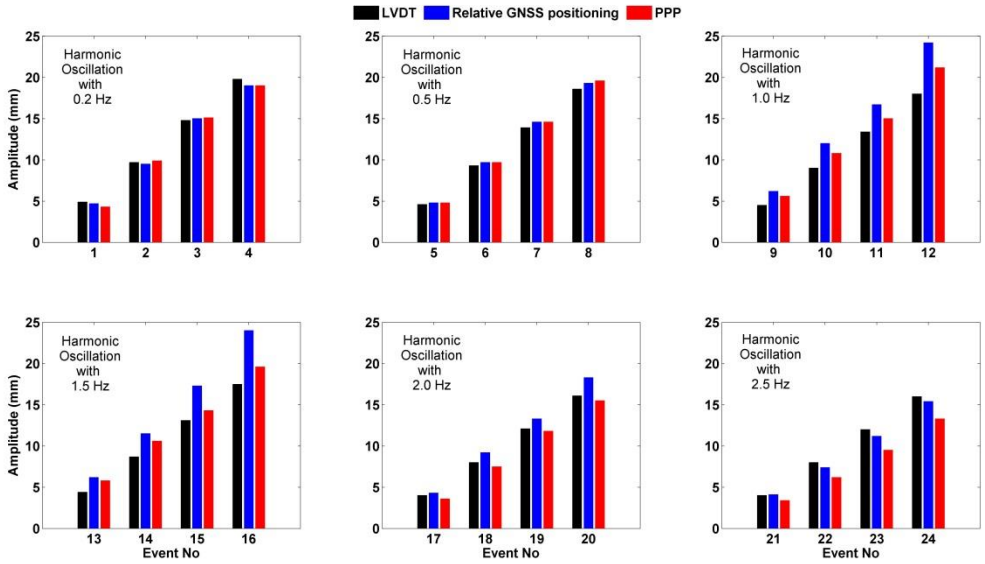

Figure 7. Amplitude of peak frequency for all events for LVDT (left), Relative GNSS positioning (middle), and PPP (right).

To compare the three methods in the time domain, the displacements obtained from each method for event 7 are depicted in figure 8, as a representative example. Figure 8 also shows the histogram of the differences in displacements between relative-GNSS positioning and LVDT, as well as between PPP and LVDT for this event. These differences ranged between -4 mm and 4 mm, and approximately follow a normal distribution. These differences are mainly due to inherent GNSS noise.

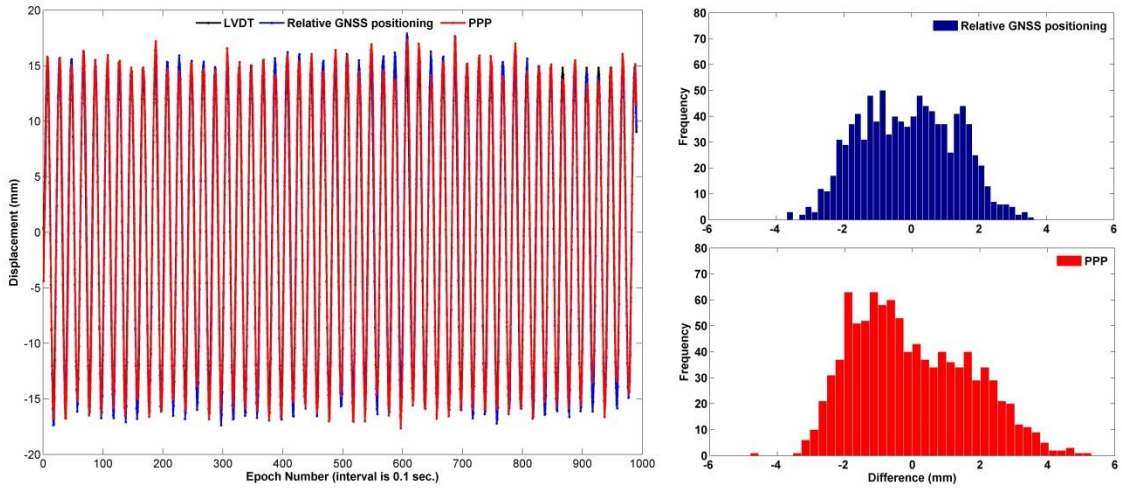

Figure 8. Comparison of PPP, relative GNSS positioning and LVDT-derived displacement at Event 7 (left). LVDT data are down-sampled to 10 Hz. Histograms of the differences between relative-GNSS and LVDT (top right) and between PPP and LVDT (bottom-right).

Harmonic oscillation tests demonstrated that the PPP method are potentially an ideal method in determining the natural frequencies of engineering structures in case where the reference GNSS station data is unavailable or unreliable for relative GNSS positioning.

4.2 Results of the El-Centro Earthquake Simulation test

Figure 9 presents the time series of displacement caused by simulating the selected record of the El-Centro earthquake. The figure shows comparisons between three methods. It can be seen that the displacement waveforms estimated from PPP, relative GNSS positioning and LVDT are largely consistent in terms of capturing the dynamic ground motion. The differences in the displacement waveform between PPP and LVDT are slightly larger than those of relative GNSS positioning and LVDT.

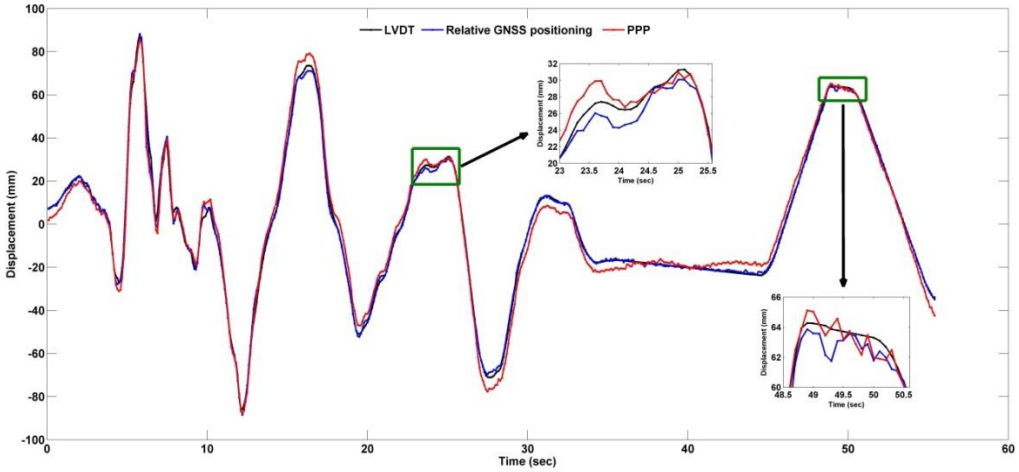

Figure 9. Comparison of PPP, relative GNSS positioning and LVDT-derived displacement at El-Centro Earthquake simulation. LVDT data are down-sampled to 10 Hz.

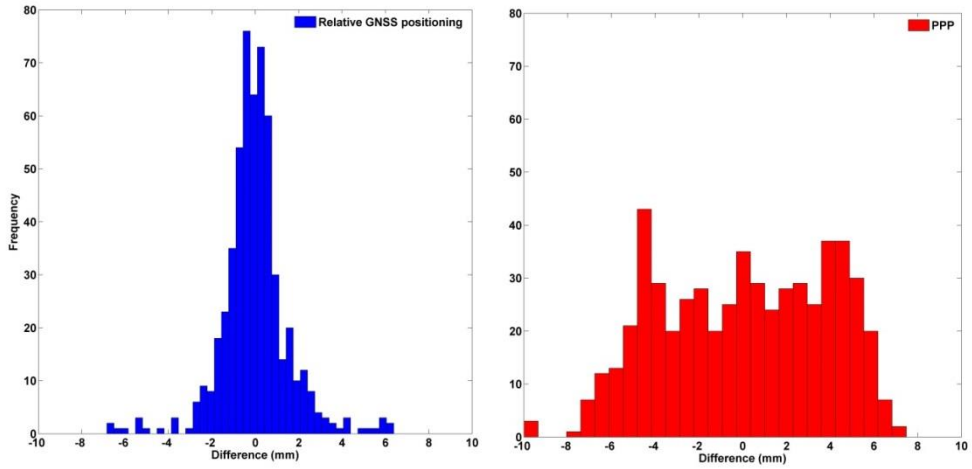

Figure 10. Histograms of the differences between relative GNSS positioning and LVDT displacement, and between PPP and LVDT-derived displacement for the El-Centro earthquake simulation

To further investigate the dynamic performance of GNSS methods, the histogram of the differences in displacements between relative GNSS positioning and LVDT, as well as PPP and LVDT are shown in figure 10. It can be seen that the displacement waveforms from PPP differ those from LVDT within -8 to 8 mm, while the displacement waveforms from relative GNSS positioning differ from those of LVDT to within -4 to +4 mm. The error distribution of relative positioning and LVDT appear to be normal, resembling a bell curve with a large concentration of samples around the mean value. The differences between PPP and LVDT are slightly larger than those of relative positioning and LVDT, which may indicate that the noise level of relative positioning is smaller than PPP.

5. ONCLUSION

In this study, large number of harmonic oscillation experiments and the El-Centro earthquake simulation experiment using shake table were performed. The performance of the relative post-mission kinematic GNSS positioning and kinematic PPP method based on twenty four harmonic oscillation events and one earthquake simulation event has been assessed through a comparison with that of LVDT data in the time and frequency domain. The shake table experiment demonstrated good agreement between LVDT, the relative GNSS positioning and PPP-derived spectrum. In general, the displacement waveforms estimated from PPP and LVDT are largely consistent in the dynamic component within a few millimeters. The results of the experiments show that the PPP method is very efficient and can satisfy structural health monitoring (SHM) and seismogeodesy applications as well as relative positioning method in terms of extracting dynamic oscillation frequencies after removing lower frequency component from PPP-derived time series. In conclusion, the PPP method are potentially an ideal method in determining the natural frequencies of engineering structures, if the reference GNSS station data is unavailable or unreliable, and earth surface wave motion caused by large earthquake.

6. ACKNOWLEDGEMENT

The first author is awarded a grant by The Scientific and Technological Research Council of Turkey (TUBITAK) to perform a research on High-rate GNSS-PPP Method for GNSS-seismology and Structural Health Monitoring Applications at School of Earth and Planetary Sciences, Curtin University, Australia. The first author would like to thank TUBITAK, Science fellowships and Grant Programmes Department for the support.

REFERENCES

Avallone A, Marzario M, Cirella A, Piatanesi A, Rovelli A, Di Alessandro C, D'Anastasio E, D'Agostino N, Giuliani R, Mattone M (2011) Very high rate (10 Hz) GPS seismology for moderate-magnitude earthquakes: the case of the Mw 6.3 L'Aquila (central Italy) event. J Geophys Res. 116:1–14.

Bilich A, Cassidy JF, Larson KM (2008) GPS seismology: application to the 2002 Mw7.9 Denali fault earthquake. Bull. Seismol. Soc. Am. 98 (2):593–606.

Bisnath S, Gao Y. (2008) Current State of Precise Point Positioning and Future Prospects and Limitations. International Association of Geodesy Symposia. 133:615-623.

Bock Y, Melgar D, Crowell BW (2011) Real-time strong-motion broadband displacements from collocated GPS and accelerometers. Bull. Seismol. Soc. Am. 101 (6): 2904–2925.

Bock Y, Prawirodirdjo L, Melbourne TI (2004) Detection of arbitrarily large dynamic ground motions with dense high-rate gps network. Geophys. Res. Lett. 31:l06604.

Cai C (2009) Precise Point Positioning Using Dual-Frequency GPS and GLONASS Measurement [Master Thesis]. Calgary: University of Calgary.

Calais E, Han JY, Demets C, Nocquet JM (2006) Deformation of the North American plate interior from a decade of continuous GPS measurements. J Geophys Res. 111:1–23.

Chan WS, Xu YL Ding XL, Xiong YL, Dai WJ. (2006) Assessment of dynamic measurement accuracy of GPS in three directions. J Surv Eng-ASCE. 132:108–117.

Çelebi M (2000) GPS in dynamic monitoring of long-period structures. Soil Dyn Earthquake Eng. 20:477–483.

El-Mowafy A, Deo M, Kubo N (2017) Maintaining real-time precise point positioning during outages of orbit and clock corrections. GPS Solut. 21:937-947.

El-Mowafy, A. (2018). Real-Time Precise Point Positioning Using Orbit and Clock Corrections as Quasi-Observations for Improved Detection of Faults. *J. of Navigation*, http://doi.org/10.1017/S0373463317001023

Ge L, Han S, Rizos C, Ishikawa Y, Hoshiba M, Yoshida Y (2000) GPS seismometers with up to 20 Hz sampling rate. Earth Planets Space 58:881–884.

Guo A,Wang Y, Li Z, Ni S,WuW, Liu G, Zheng Y, Simons M (2013) Observation of core phase ScS from the Mw9.0 Tohoku-Oki earthquake with high-rate GPS. Seismol. Res. Lett. 84 (4), 594–599.

Hung HK, Rau RJ, (2013) Surfacewaves of the 2011 Tohoku earthquake: Observations of Taiwan's dense high-rate GPS network. J. Geophys. Res. 118:332–345.

Kaloop MR, Yigit CO and Hu JH (2018) Analysis of the dynamic behavior of structures using the high-rate GNSS-PPP method combined with a wavelet-neural model: Numerical simulation and experimental tests. Advances in Space Research, https://doi.org/10.1016/j.asr.2018.01.005

Kouba J, Hérou P (2001) Precise Point Positioning using IGS orbit and clock products. GPS Solutions. 5:12–28.

Kouba J (2003) Measuring seismic waves induced by large earthquakes with GPS. Stud Geophys Geod. 47:741–755.

Larson KM, Bodin P, Gomberg J (2003) Using 1-Hz GPS data to measure deformations caused by the Denali fault earthquake. Science 300:1421–1424.

Li X, Ge L, Ambikairajah E, Rizos C, Tamura Y, Yoshida A (2006) Full-scale structural monitoring using an integrated GPS and accelerometer system. GPS Solutions. 10:233–247.

Li X, Ge M, Zhang X, Zhang Y, Guo B, Wang R, Klotz J, Wickert J (2013) Real-time high-rate co-seismic displacement from ambiguity-fixed Precise Point Positioning: application to earthquake early warning. Geophys Res Lett. 40:295–300.

Michel C, Kelevitz K., Houlié N, Edwards B, Su Z, Clinton J, & Giardini D (2017) The Potential of High-Rate GPS for Strong Ground Motion Assessment, 107 (4): 1849-1859.

Moschas F, Avallone A, Saltogianni V, Stiros SC (2014) Strong motion displacement waveforms using 10-Hz precise point positioning GPS: an assessment based on free oscillation experiments. Earthquake Eng Struct Dyn. 43:1853–1866

Moschas F, Stiros SC (2014) Three-dimensional dynamic deflections and natural frequencies of a stiff footbridge based on measurements of collocated sensors. Struct Control Health Monit. 21:23–42.

Nakamura S (2000) GPS measurement of wind-induced suspension bridge girder displacements. J Struct Eng-ASCE. 126:1413–1419.

Nie Z., Zhang R, Liu G, Jia Z, Wang D, Zhou Y, & Lin M (2016) GNSS seismometer : Seismic phase recognition of real-time high-rate GNSS deformation waves. Journal of Applied Geophysics, 135, 328–337.

Ohta Y, Ohzono M, Miura S, Iinuma T, Tachibana K, Takatsuka K, Miyao K, Sato T, Umino N (2008) Coseismic fault model of the 2008 Iwate-Miyagi Nairiku earthquake deduced by a dense GPS network. Earth Planets Space. 60:1197–1201.

Park HS, Sohn HG, Kim IS, Park JH (2008) Application of GPS to monitoring of wind-induced responses of high-rise buildings. Struct Des Tall Spec Build. 17:117–132.

Psimoulis PA, Stiros SC (2008) Experimental assessment of the accuracy of GPS and RTS for the determination of the parameters of oscillation of major structures. Comput-Aided Civil Infrastructure Eng. 23:389–403.

Roberts GW, Meng X, Dodson A (2004) Integrating a global positioning system and accelerometers to monitor deflection of bridges. J Surv Eng. 130:65–72.

Savage JC, Gan W, Prescott WH, Svarc JL (2004) Strain accumulation across the coast ranges at the latitude of San Francisco, 1994–2000. J Geophys Res. 109:1–11.

Shi C, Lou Y, Zhang H, Zhao Q, Geng J, Wang R, Fang R, Liu J (2010) Seismic deformation of the Mw8.0 Wenchuan earthquake from high-rate GPS observations. Adv. Space Res. 46:228–235.

Wang G, Blume F, Meertens C, Ibanez P, Schulze M (2011) Performance of high-rate kinematic GPS during strong shaking: observations from shake table tests and the 2010 Chile earthquake. J Geodetic Sci. 2:1–15.

Xu P, Shi C, Fang R, Liu J, Niu X, Zhang Q, Yanagidani T (2013) High-rate precise point positioning (PPP) to measure seismic wave motions: an experimental comparison of GPS PPP with inertial measurement units. J Geod. 87:361–372.

Yi J, Zhang JW, Li QS (2013) Dynamic characteristics and wind-induced responses of a super-tall building during typhoons. J Wind Eng Ind Aerodynamics. 121:116–130.

Yi T, Li H, Gu M (2013) Experimental assessment of high-rate GPS receivers for deformation monitoring of bridge. Measurement. 46:420–432.

Yigit CO, Li X, Inal C, Ge L, Yetkin M (2010) Preliminary evaluation of precise inclination sensor and GPS for monitoring full-scale dynamic response of a tall reinforced concrete building. J Appl Geod. 4:103–113.

Yigit CO (2016) Experimental assessment of post processed kinematic precise point positioning method for structural health monitoring. Geomat Nat Hazards Risk. 7:363–380.

Yigit CO and Gurlek E (2017) Experimental testing of high-rate GNSS precise point positioning (PPP) method for detecting dynamic vertical displacement response of engineering structures Geomat., Nat. Haz. Risk, 8(2): 893-904.

Yin HT, Wdowinski S, Liu X, Gan WJ, Huang B, Xiao G, Liang S (2013) Strong ground motion recorded by high-rate GPS of the 2008 Ms8.0 Wenchuan. Seismol. Res. Lett. 84 (2):210–218.

Zumberge JF, Heflin MB, Jefferson DC, Watkins MM, Webb FH (1997) Precise Point Positioning for the efficient and robust analysis of GPS data from large networks. J Geophys Res. 102:5005–5017.

BIOGRAPHICAL NOTES

Cemal Ozer Yigit is an Associate Professor in the Department of Geomatics Engineering at Gebze Technical University, Gebze, Turkey. He holds a Doctor of Philosophy degree and Master of Science in Geomatics from Selcuk University, Turkey. His current research interests include high-rate GNSS PPP, precise positioning, crustal deformation monitoring, seismogeodesy, structural health monitoring, and deformation analysis.

Ahmet Anil Dindar is an Assistant Professor in the Department of Civil Engineering at Gebze Technical University, Gebze, Turkey. He holds a Doctor of Philosophy degree from Bogazici Univertsity, Turkey, and Master of Science in Civil Engineering from Istanbul Technical University, Turkey. His current research interests involve structural health monitoring, energy-based reinforced concrete structure analysis and design, dynamic testing systems.

Mert Bezcioglu is a Research Assistant in the Department of Geomatics Engineering at Gebze Technical University, Gebze, Turkey. He is currently a Master student at Gebze Technical University.

Ahmed El-Mowafy is an Associate Professor and Director of Graduate Research, School of Earth and Planetary Sciences, Curtin University, Australia. He holds a Doctor of Philosophy degree from the University of Calgary, Canada, and a Bachelor of Science in Civil Engineering and Master of Science in Surveying and Geodesy from Ain Shams University, Egypt. His main areas of research are integrity monitoring and quality control of GNSS applications, precise positioning and navigation, attitude determination, integration of GNSS with other sensors, deformation analysis, and hydrographic surveying.

CONTACTS

Cemal Ozer YIGIT
Associate Professor
Department of Geomatics Engineering
Gebze Technical University

Gebze 41400
TURKEY
Tel. +90 216 605 18 07
Fax + 90 216 605 18 05
Email: cyigit@gtu.edu.tr
Web site: http://orcid.org/0000-0002-1942-7667

Ahmet Anil DINDAR
Assistance Professor
Department of Civil Engineering
Gebze Technical University
Gebze 41400
TURKEY
Tel. +90 216 605 33 10
Fax + 90 216 653 83 90
Email: adindar@gtu.edu.tr
Web site: http://www.a2d.co/

Mert BEZCIOGLU
Research Assistant
Department of Geomatics Engineering
Gebze Technical University
Gebze 41400
TURKEY
Tel. +90 216 605 18 13
Fax + 90 216 605 18 05
Email: mbezcioglu@gtu.edu.tr
Web Site: http://www.gtu.edu.tr/

Ahmed EL-MOWAFY
Associate Professor
Spatial Science
School of Earth and Planetary Sciences
Curtin University
Perth WA 6845
AUSTRALIA
Tel. +61 8 9266 3403
Fax + 61 8 9266 2703
Email: A.El-Mowafy@curtin.edu.au
Web site: http://orcid.org/0000-0001-7060-4123